The importance of resonance and potential vorticity unshielding to the evolution of optimal perturbations

Hylke de Vries[1]*, Theo Opsteegh[2]

[1] *Institute for Marine and Atmospheric Research Utrecht, Utrecht University, Utrecht, The Netherlands*

[2] *Royal Netherlands Meteorological Institute, De Bilt, The Netherlands*

February 3, 2004

ABSTRACT

Using a nonmodal decomposition technique based on the potential vorticity (PV) perspective the optimal perturbation or singular vector (SV) of the Eady model without upper rigid lid is calculated for different kinetic energy norms. It is found that PV anomalies which reside above the steering level of the surface edge wave and are in (near) linear resonance with the latter are very important to drive the SV's surface cyclogenesis.

In the PV perspective the SV is formed by a set of PV anomalies residing at horizontal levels and by surface potential temperature (PT) anomalies rather than by a number of normal modes. The analytical, nonmodal approach has two important advantages as compared to a standard modal approach. First, it avoids the singularity problem which occurs if continuum modes (neutral normal modes associated with both interior PV and boundary PT) in the vicinity of the steering level of the edge wave are retained. This steering level is important because the system is resonantly unstable to PV perturbations at this level. In a numerical, modal approach the resonant mode is not included. The second advantage is that the nonmodal approach allows the SV to be reconstructed step by step. One can start with one PV anomaly in the interior and include more PV anomalies thereafter. In this way the complexity is increased step by step as well. This is not possible with a modal approach.

With one PV anomaly in the initial PV-distribution, the SV growth is dominated by the aforementioned resonance except for small optimization times (less than one day) in which case unshielding of PV and surface PT dominate the growth of the SV. For all optimization times PV-PT unshielding provides additional growth to the SV and this explains the observation that the PV is located always above the resonant level. More PV anomalies are added to the initial perturbation to include PV-unshielding as a

* *Corresponding author address:* Hylke de Vries. E-mail: h.devries@phys.uu.nl

third growth mechanism and it is found that the relative importance of the three mechanisms depends both on the optimization time and on the number of PV anomalies used in the initial perturbation. When PV is allowed at more than two interior levels, PV unshielding becomes the dominant growth mechanism for the interior of the perturbation and PV-PT unshielding even contributes negatively to the SV's amplitude. At the surface resonance plays still a dominant role even when a total kinetic energy norm is used. Furthermore we observe, in agreement with a recent paper by Kim and Morgan, that the PV distribution becomes increasingly more concentrated near the steering level of the edge wave for increasing optimization times. This concentration of PV near the steering level is explained in more detail using the concept of resonance.

1. Introduction

For more than a century there has been interest in extratropical surface cyclogenesis and its underlying dynamics. One of the first analytical approaches to cyclogenesis appeared in 1949. Based on the observed mean flow at midlatitudes Eady (1949) constructed a linearized quasigeostrophic model. The basic state is provided by an inviscid shear flow between two horizontal rigid lids representing the earth surface and the tropopause. Eady showed that the background atmospheric flow is exponentially unstable to long-wave perturbations. These unstable normal modes have zero interior quasigeostrophic potential vorticity (PV from here) and hence are purely thermal edge waves.

Ever since the pioneering work of Eady, researchers have looked for different growth mechanisms to explain the observed behaviour of developing cyclones. Pedlosky (1964) solved the initial value problem for the Eady model in complete generality and showed that there is another class of disturbance structures supported by the background flow. These so-called continuum modes (CM) are characterized by both a singular perturbation of PV at some interior level and a nonzero potential temperature structure at the boundaries. It is only with the help of this infinite number of CMs that the finite-time dynamics of an arbitrary initial disturbance is correctly represented. The observation that transient effects of superposition can result in remarkable perturbation growth is not new and dates back to the work of Orr (1907). Farrell (e.g. Farrell 1982; Farrell 1984; Farrell 1988; Farrell 1989) has been among the first to explicitly show that the CMs can play an important role in the cyclogenesis problem. The basic question Farrell addressed is the following: what is the structure of the initial perturbation, such that for a given basic state the perturbation linearly amplifies most rapidly for a given norm over a prescribed time interval? These optimal perturbations are called singular vectors (SV). Farrell showed that the finite-time rapid baroclinic amplification of a favorably configured initial disturbance can exceed the growth due to normal mode instability. While eventually the growing normal mode

becomes important, the initial growth is dominated by what is nowadays called nonmodal wave growth. Here, a nonmodal disturbance is defined as any disturbance structure that comprises more than one single mode (Farrell 1984). Nowadays SVs are calculated for all types of models including NWP models using numerical methods. On a weather map the SV appears as a very localized structure and it gives an indication of the location where future development is to be expected, and where forecast errors may grow rapidly. Because of this signaling function, it is worthwhile to understand the SV in terms of the underlying dynamics.

Most analytical studies on singular vectors for the Eady model concentrate on the growing normal modes and leave the CMs out of consideration. Rotunno and Fantini (1989) studied optimal perturbations created by superposition of growing normal modes of one fixed wavelength. Their analytical work then has been extended to include variable wavenumbers by Fischer (1998). Much less is known about the fact that the CM can generate sustained perturbation growth as well. If the PV of a CM is located exactly at the steering level of one of the edge waves, an edge wave is resonantly excited and the perturbation streamfunction grows linearly in time. The existence of a linear resonance has been found before in analytical studies of the Eady model where the upper rigid lid was removed (Thorncroft and Hoskins 1990; Chang 1992; Davies and Bishop 1994; Bishop and Heifetz 2000) but no serious attempt has been made sofar to include the impact of the linear resonance in an analytical approach to the SV. To fill the gap we will concentrate on the role of the CMs in the SV structure and especially on the importance of resonance in the SV evolution. This is done using an analytical treatment of the semi-infinite Eady model. The results will be compared with the existing literature on short-wave numerical SV analyses, to be summarized below.

Although the CM is ignored in the analytical studies, the CMs have been included in most numerical approaches. Farrell (1988) has been the first to calculate the SV for simplified atmospheric models using streamfunction variance (L2) and total kinetic energy as a norm. He finds optimal perturbations having a PV distribution which is initially tilted extremely upshear. These results are confirmed and worked out for the Eady model in more detail by Mukougawa and Ikeda (1994). Hakim (2000) studied the evolution of an upperlevel PV anomaly and found that the growth due to unstable normal modes is more important than SV growth. Similarly, Badger and Hoskins (2001) studied the dynamics of a spatially localized vortex but they noticed that so-called PV-unshielding plays an important role in the initial stage of the development. The effect of growth due to linear resonance is not explicitly considered in these numerical studies.

The CM can only yield linear resonance in the Eady model, if the wavenumber of the perturbation is large enough to guarantee a steering level within the flow domain. Let us therefore focus on the short-wave SVs in the numerical approaches to the SV in the Eady model. Morgan (2001) and Morgan and Chen (2002)

analyzed the Eady model SV for the L2-norm using two different numerical partitionings of the SV. A brief discussion of both partitionings is given below and serves to clarify pro's and contra's of both approaches.

The first is a modal partitioning. The SV streamfunction ψ_{sv} is divided into an Eady edge wave part, ψ_{nm} and a continuum mode part ψ_{cm}. The advantage of this partitioning is clear. Modal solutions do not change their structure with time. However, there is also a disadvantage. As a result of the necessary constraints at horizontal rigid surfaces, the streamfunction of the CM becomes nearly singular if the potential vorticity is located near the steering level of the neutral edge wave, which makes it difficult to address the optimization problem numerically. This may be a motivation to choose for a potential vorticity partitioning. In this PV-based partitioning (Morgan 2001), the streamfunction is decomposed into an interior PV part, ψ_{pv}, and a part that is associated with the potential temperature anomalies at the horizontal boundaries ψ_θ. The advantage of this approach is that it is physically transparent. However, the individual parts now evolve in a nonmodal way, which may be a disadvantage for a clear understanding.

Analysing the short-wave SV evolution resulted in the following schematic three-stage development (Morgan 2001): 1) a superposition of interior PV anomalies, 2) a subsequent intensification of the boundary potential temperature anomalies due to the advection of background potential temperature gradient by the winds associated with interior PV, 3) finally a transient interaction between the upper and lower boundary potential temperature anomalies. The observations of Morgan (2001) have been analysed and confirmed by Morgan and Chen (2002). They confirm the important role of initial masking and subsequent unshielding of the Eady edge modes by the CMs in the evolution of the SV. They observe that for the short-wave perturbations, only a small number of CMs is required to mask the edge modes.

The work of Morgan (2001) and Morgan and Chen (2002) has been generalized and reconsidered by Kim and Morgan (2002) using both a total quasigeostrophic energy norm and a potential enstrophy norm. From their work it is concluded that the choice of norm may influence the result substantially. It depends on the specific choice whether 1), 2), or 3) of the above mentioned three-stage SV evolution dominates. Furthermore, in Morgan and Chen (2002) and Kim and Morgan (2002) the length of the optimization time is varied and it is found that for increasing optimization time, the importance of the PV near the steering levels of the edge waves becomes more important for shortwave perturbations. The explanation they give for this PV-concentration is that it allows for a longer near-resonant interaction between the PV and the edge wave.

In the present paper we will investigate the analytical structure of the SV of the Eady model with an emphasis on the importance of resonance effects and PV unshielding. In order to extend the existing literature on analytically constructed optimal perturbations (Rotunno and Fantini 1989; Fischer 1998), we will keep the CMs included. To quantify the importance of resonance for the surface dynamics, we use the semi-infinite

version of the Eady model as formulated by Thorncroft and Hoskins (1990). The surface dynamics of this model resembles the surface dynamics of the conventional Eady model above the instability cutoff.

In section 2, the semi-infinite version of the Eady model is introduced, with special emphasis on the continuous spectrum. In section 3 a PV-basis is constructed with the help of nonmodal building blocks. These building blocks consist a superposition of one CM and one edge wave with initially zero surface potential temperature. This PV-basis is used in section 4 to construct the SV, starting with the optimal position for one PV building block. In section 5 the generalization towards a general distribution of potential vorticity is considered Section 6 consists of a summary of the main conclusions and finally an appendix is added to clarify a subtle point in the numerical scheme.

2. Equations and normal mode solutions

The basic equation that governs the dynamics of the Eady model without upper rigid lid is the conservation of quasigeostrophic potential vorticity (PV) q

$$\left(\frac{\partial}{\partial t} + \bar{U}\frac{\partial}{\partial x}\right) q(x,y,z,t) = 0, \tag{1}$$

where $\bar{U} = \Lambda z$ is the basic zonal flow, y the meridional direction, x the zonal direction, z the vertical direction and t time. The basic state is assumed to have zero interior PV and Λ has a typical value of 3 ms^{-1} per km height, which is characteristic for the mid-latitudes. q is related to the perturbation streamfunction ψ by:

$$q(x,y,z,t) = \left(\frac{\partial^2}{\partial x} + \frac{\partial^2}{\partial y} + \frac{1}{S^2}\frac{\partial^2}{\partial z^2}\right)\psi(x,y,z,t). \tag{2}$$

with $S^2 := (N_0 D)^2 (f_0 L)^{-2}$ the stratification parameter or Burger number which in the present study is of order unity. Variables have been nondimensionalized using the scalings $(L, H, L/U, f_0 LU)$ where $L = NH/f_0 \sim 10^6 m$ scales the horizontal coordinates x and y and $H \sim 10^4 m$ scales the vertical coordinate z. $L/U \sim 9,26h$ is the characteristic time-scale, and $f_0 LU \sim 3 \cdot 10^3 m^2 s^{-2}$ scales the geostrophic streamfunction. Furthermore, $U \sim 30 ms^{-1}$ and finally a constant Coriolis parameter $f_0 \sim 10^{-4} s^{-1}$ is assumed as well as a constant buoyancy frequency $N_0^2 \sim 10^{-4} s^{-2}$. Wavenumbers of the perturbations have been nondimensionalized as well and a nondimensional zonal wavenumber $k = 1$ corresponds with a physical wavelength of 6280 km.

At the earth surface the condition that the vertical velocity equals zero leads to

$$\left(\frac{\partial}{\partial t} + \bar{U}\frac{\partial}{\partial x}\right)\frac{\partial \psi}{\partial z} - \frac{\partial \bar{U}}{\partial z}\frac{\partial \psi}{\partial x} = 0 \quad (z = 0), \tag{3}$$

where $\partial\psi/\partial z \equiv \theta$ defines the potential temperature. As a scaling for the potential temperature, we choose $(ULf_0 g^{-1} H^{-1})\Theta_{00} = 9.18K$, for a given reference potential temperature $\Theta_{00} = 300K$ and $g = 9.81 ms^{-2}$ the gravity constant. For consistency, it is required that the perturbation streamfunction vanishes at infinite

height. Because $\bar{U} = 0$ at the earth surface, (3) implies an exact balance between the tendency of the local perturbation potential temperature $\partial\theta/\partial t$ and the horizontal advection of mean temperature by the perturbation meridional velocity $\Lambda\partial\psi/\partial x$.

At the vertical boundaries, we have vanishing of the meridional velocity $v = \partial\psi/\partial x = 0$. From now on, we will neglect the influence of these vertical boundaries and study perturbations which are homogeneous in the meridional direction. This is done by choosing a meridional wavenumber equal to zero. Although this choice is formally not correct, it does not alter the results to be presented below significantly.

a. Eady edge wave

Modal solutions for the Eady model without upper rigid lid come in two classes, with zero and nonzero interior PV. We treat them separately because of the differences in vertical structure. Solving (1) and (3) for $q = 0$ we obtain the streamfunction of the Eady edge wave

$$\psi^{nm}(x, z, t) = e^{-\mu z} \sin(k(x - \frac{\Lambda}{\mu}t)), \tag{4}$$

where $\mu = S(k^2 + l^2)^{1/2} = 1/H_R$ defines the inverse Rossby height. Due to the absence of the upper rigid boundary, the Charney-Stern condition for instability is not satisfied and the solution is a baroclinically stable oscillation that propagates zonally with the speed of the basic state flow at one Rossby height above the surface.

b. Continuum modes

For the semi-infinite Eady model, there exists an infinite number of neutral normal modes, called continuum modes (CM). These modes are associated with nonzero PV at some level h in the interior of the flow:

$$q(x, z, t) = Q\delta(z - h) \sin(k(x - \Lambda ht)), \tag{5}$$

with Q the amplitude of PV. Notice that $q(x, z, t) = q(x - \Lambda ht, z, 0)$ due to PV conservation. The streamfunction of the CM has been calculated by Thorncroft and Hoskins (1990). For $h \neq 1/\mu$, the streamfunction reads

$$\begin{aligned} \psi^{cm}(x, z, t) &= \underbrace{\frac{S^2Q}{\mu}\left(H(z - h)\sinh\mu(z - h) - e^{-\mu h}\cosh\mu z\right)\sin(k(x - \Lambda ht))}_{\psi^{cm}_{pv}(x,z,t)} \\ &+ \underbrace{\frac{S^2Q}{\mu}\left(\frac{e^{-\mu h}}{1 - \mu h}\right)e^{-\mu z}\sin(k(x - \Lambda ht)}_{\psi^{cm}_{\theta}(x,z,t)}, \end{aligned} \tag{6}$$

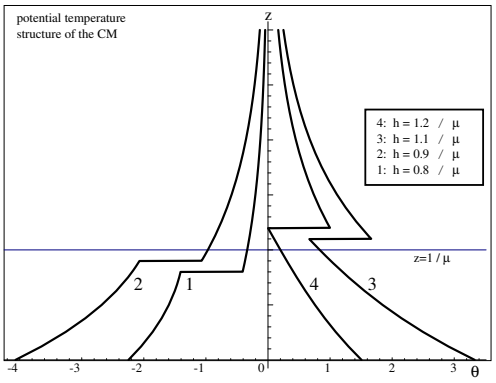

Fig. 1: Potential temperature structure of the continuum mode as a function of height z for different values of h and a positive value of the PV.

where $H(z-h)$ is the Heavyside stepfunction[1]. The streamfunction ψ^{cm} has been partitioned into a potential temperature (PT) part ψ^{cm}_{θ} and a potential vorticity (PV) part ψ^{cm}_{pv}. In this PV partitioning, ψ^{cm}_{θ} is that part of the streamfunction which is purely associated with anomalous surface PT, but not with interior PV. Similarly, ψ^{cm}_{pv} is that part of ψ^{cm} with zero surface PT, but nonzero PV. This notation is due to Morgan and Chen (2002) and will be used throughout the paper:

$$\left(\frac{1}{S^2}\frac{\partial^2}{\partial z^2} - \mu^2\right)\psi_{pv} = q, \quad \left(\frac{\partial \psi_{pv}}{\partial z}\right)\Big|_{z=0} = 0 \tag{7}$$

$$\left(\frac{1}{S^2}\frac{\partial^2}{\partial z^2} - \mu^2\right)\psi_{\theta} = 0, \quad \left(\frac{\partial \psi_{\theta}}{\partial z}\right)\Big|_{z=0} = \theta|_{z=0}. \tag{8}$$

Observing the streamfunction of the CM, it is immediately clear that the temperature part ψ^{cm}_{θ} in (6) has the same vertical structure as the edge wave (4) but a different propagation speed. Furthermore, the amplitude of ψ^{cm}_{θ} becomes arbitrarily large when h approaches the steering level of the neutral edge wave. The PT-structure of the CM is displayed in Fig. 1 for various values of the height h. This figure shows that a CM located above $1/\mu$ has an anomalously warm surface PT, while a CM located below $h = 1/\mu$ has an anomalously cold surface PT.

The sign and amplitude of ψ^{cm}_{θ} at the surface depend on the height of the PV anomaly. This is a result from the thermodynamic equation (3). In terms of the PV-partitioning the thermodynamic equation reads

$$\left(\frac{\partial^2}{\partial t \partial z} - \frac{\partial \bar{U}}{\partial z}\frac{\partial}{\partial x}\right)\psi^{cm}_{\theta} = \left(\frac{\partial \bar{U}}{\partial z}\frac{\partial}{\partial x}\right)\psi^{cm}_{pv}, \quad (\text{at } z = 0). \tag{9}$$

The boundary condition at $z = 0$ implies a balance between three processes. At the rhs of (9) we have the meridional advection of basic state potential temperature by the winds due to ψ^{cm}_{pv}. For a modal structure,

[1]Precise readers may convince themselves of the difference with the continuum mode found in the existing literature on resonant modes. In Thorncroft and Hoskins (1990) as well as in Chang (1992) a factor $\exp(-\mu h)$ is erroneously omitted.

the potential temperature perturbation that is the result of this advection, should propagate with the same speed as the PV. It is important to realize that for $h \neq 1/\mu$ this speed is not equal to the propagation speed of the surface Eady edge wave. It is easily verified that for $h < 1/\mu$, the advection of mean potential temperature exceeds the tendency of the local perturbation potential temperature due to ψ_θ. The thermodynamic constraint gives a relation between the signs of interior PV and surface potential temperature. More specifically, the sign of the potential temperature must be of the opposite (same) sign of Q when $h < 1/\mu$ ($h > 1/\mu$).

From the PV-partitioning, it is clear that the amplitude of the total streamfunction will get arbitrarily large when h approaches the steering level of the Eady edge wave. In this situation, the lhs of (9) almost vanishes, and the amplitude of the surface thermal wave ψ_θ^{cm} increases to satisfy (9).

At $h = 1/\mu$ exactly, a linear resonance occurs because the PV anomaly and the edge wave move at the same speed and the lhs of (9) would vanish for a constant amplitude ψ_θ^{cm}. Straightforward solving the equations leads to the result of Thorncroft and Hoskins (1990):

$$\psi^{cm}(x,z,t) = \psi_{pv}^{cm}(x,y,z,t) + \underbrace{S^2 Q \frac{\Lambda k t}{\mu^2} e^{-\mu(z+h)} \cos(k(x - \frac{\Lambda}{\mu}t))}_{\psi_{\theta,res}^{cm}(x,z,t)}, \tag{10}$$

with initial condition $\theta(z = 0, t = 0) = 0$ and where ψ_{pv}^{cm} is the same as in (6). The amplitude of the thermal part of the streamfunction increases linearly in time and is a quarter of a wavelength out of phase with ψ_{pv}^{cm}, which is the expected phase relation (Davies and Bishop 1994). Remark that this resonance exists for all values of the wavenumber k because the steering level of the Eady edge wave always lies in the physical domain.

3. A nonmodal PV-basis for initial-value experiments

The discussion of the different modal solutions to the system of equations illustrates the importance of boundary conditions in PV dynamics. Although the dynamics of the PV anomaly itself is rather trivial (it is advected by the basic flow), the wind fields in the vicinity of the PV anomaly of a CM do not necessarily agree with standard PV thinking (Hoskins et al. 1985), especially for the near-resonant CM. The question rises whether or not in an analytical approach to the SV of the Eady model we can include the CMs without having to deal with the very large surface potential temperatures of the near-resonant CMs.

From (6) it is clear that the singular behaviour of the CM near the steering level is exclusively caused by the thermal part ψ_θ^{cm}. This part of the CM shows the same exponential decay with height as the edge wave with the same wavelength. So it makes sense to build up the initial PV-distribution of the SV with couplets of CM and associated edge wave in such a way that the initial surface potential temperature is zero

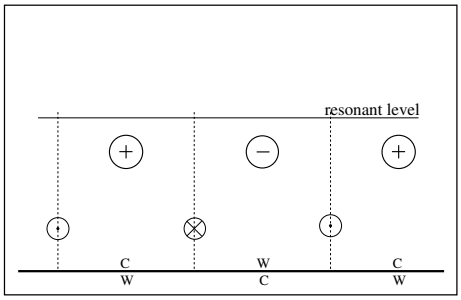

Fig. 2: Basis function in the PV-basis. ψ_θ^{cm} of a CM below the resonant level is masked by an edge wave with opposite amplitude. The PV anomalies are indicated by the encircled plus and minus signs. The wind fields due to the PV anomalies are represented by an encircled cross (northward) and dot (southward). Finally, the PT structure of the CM / edge wave is indicated with the w and c signs just above / below the surface.

(see Fig. 2 for a schematic representation). Due to the differences in propagation speed of edge wave and CM, a surface potential temperature wave is generated as time increases. It is easily verified that as a result of this superposition, the problem with the singularity is automatically postponed to $t = \infty$.

It is known that the complete QG-flow is determined by the distribution of interior PV and boundary potential temperature (Hoskins et al. 1985). That is, the CM-edge wave couplets together with the edge waves can be used as building blocks to form a PV-basis for perturbations with any initial distribution of interior PV and surface PT. Two advantages of this approach are immediately clear. First, the resonant mode is retained and second, the singular behavior of the near-resonant modes has been removed in a simple way. Moreover, the nonmodal approach allows a step-by-step construction of the SV. Instead of dealing with a general PV-distribution in the SV, one may start with one PV building block in the initial perturbation and search for its optimal position, i.e the height that generates the largest surface cyclogenesis at the relevant time-scale (i.e in the order of two days). This is the topic of the next section.

a. Definition of the singular vector and the norm

Singular vector perturbations are constructed to produce optimal growth in some specified norm. Common choices are L2 streamfunction norm, total QG-energy norm and potential enstrophy norm. In this paper we concentrate on the structure of the perturbation that generates the largest surface cyclogenesis and then a suitable choice seems to be the zonally integrated surface kinetic energy of the perturbation (from here called the L-norm). Given $v = \partial\psi/\partial x$, the zonally integrated surface kinetic energy $E(t)$ at time t is computed as:

$$E(t) = \int_0^{2\pi/k} \frac{v^2}{2} \mathrm{d}x \equiv \langle \psi(t), \psi(t) \rangle_L \Big|_{z=0}. \tag{11}$$

The surface kinetic energy can be written as as the correlation $\langle \psi(t), \psi(t) \rangle_L$ of the streamfunction with respect to the L-norm. The finite time growth-factor is defined as the ratio between the surface kinetic energy at initial and final time:

$$\Gamma(t) := \left. \frac{E(t)}{E(0)} \right|_{z=0}. \tag{12}$$

The next step is to vary the perturbation structure to optimize $\Gamma(t)$ for a given optimization time t. That initial perturbation structure that gives rise to a maximal $\Gamma(t)$ is called the optimal perturbation or singular vector (SV). In the next section we will calculate $\Gamma(t)$ for the streamfunction of one PV building block. As said before, at initial time this building block PV at one particular level and zero PT at the surface. We will determine the position at which this PV anomaly generates the largest growth-factor given the optimization time.

4. Optimal position of one PV anomaly

To determine the optimal height for one PV anomaly analytically, one needs the streamfunction. This streamfunction is easily obtained from the streamfunction of the CM by adding an edge wave with opposite amplitude. It reads

$$\psi(x,z,t) = \psi_{pv}^{cm}(x,z,t) + \frac{S^2 Q}{\mu} \frac{e^{-\mu(z+h)}}{1-\mu h} \left(\sin(k(x-\Lambda h t)) - \sin(k(x - \frac{\Lambda}{\mu} t)) \right). \tag{13}$$

The surface kinetic energy is calculated from the wind fields of (13) at $z = 0$. The growth-factor is then obtained as:

$$\Gamma(t) = \left(\frac{1 + \mu^2 h^2 - 2\mu h \cos(k\Lambda(h - 1/\mu)t)}{(1-\mu h)^2} \right). \tag{14}$$

Remark that this equation is independent of the amplitude of the PV-anomaly. All localized PV-anomalies of a given wavelength produce the same growth-factor. Inverting (14) to obtain the optimal height as function of the optimization time, is not possible and therefore (14) is plotted in Fig. 3 for optimization times varying between 30 and 67 hours. From this figure one observes that the maximum growth-factor is obtained if the initial PV anomaly is located *above* the resonant level. For short optimization times the exact location of the CM is less important and maximal growth-factors are obtained in a relatively broad regime above the resonant level. For larger optimization times this maximum moves asymptotically towards the resonant level and the band of optimal growth-factors narrows. In the limit of infinite optimization time the maximum growth-factor is obtained with an initial PV anomaly at the resonant level $h = 1/\mu$. The fact that it is for all times better to locate the initial PV anomaly not exactly at the resonant level, shows that both resonance and unshielding play an important role in the finite time optimization problem. In the next section we examine the importance of the various growth mechanisms during the development.

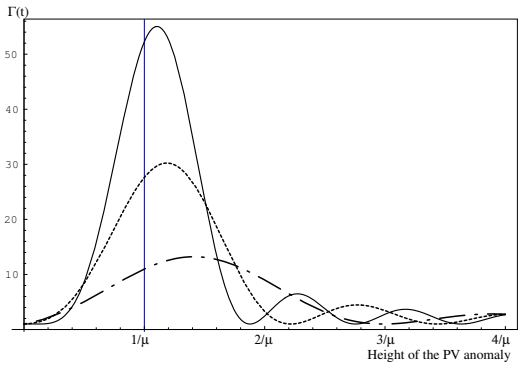

Fig. 3: Surface kinetic energy growth-factor as a function of the height of the PV anomaly for different optimization times $t_{opt} = 3.16$ (30 hours) (dash-dot), $t_{opt} = 5.16$ (two days) (dashed) and $t_{opt} = 7.16$ (67 hours) (full). The other parameters are $\Lambda = 1.0$, $k = 2.0$, $S = 1.0$.

a. projections of the SV streamfunction

The importance of the different growth mechanisms during the various stages of the development are revealed by calculating the projections of the SV streamfunction. Morgan and Chen (2002) calculated projection coefficients for their modal decomposed SV as well as for their PV-PT decomposed SV. A similar analysis is presented below. The SV streamfunction ψ_{sv} is written as a sum of a PV and a PT part, $\psi_{sv} = \psi_{pv} + \psi_{\theta}$. The different growth mechanisms that play a role during the SV evolution are then just the different correlations appearing in the following expression:

$$\frac{\langle \psi_{pv}, \psi_{pv} \rangle_L}{||\psi_{sv}||^2} + 2\frac{\langle \psi_{pv}, \psi_{\theta} \rangle_L}{||\psi_{sv}||^2} + \frac{\langle \psi_{\theta}, \psi_{\theta} \rangle_L}{||\psi_{sv}||^2} = 1.$$

The first process is PV unshielding, which clearly does not play a role when only one PV anomaly is considered. The second process is the unshielding of PV and PT. And finally we have the growing surface PT wave due to resonance. In Fig. 4 we have plotted the evolution of the various projection coefficients for the $t_{opt} = 3.16$ (30 hours) and $t_{opt} = 5.16$ (2 days) optimal building block. Initially, the SV completely projects on the PV part because there is zero surface PT. The winds due to the PV anomaly then quickly trigger a surface PT wave. This surface PT wave propagates with a slightly different propagation speed and we see that both resonance (dash-dot-dot) and PV-PT unshielding (full) contribute positively to the growth. Furthermore, we notice that for both optimization times the largest growth of the SV-amplitude is caused by the resonance and that unshielding of PV and PT plays a secondary role. However, this PV-PT unshielding mechanism becomes more important as the optimization time is decreased. For optimization times smaller than about 13 hours, PV-PT unshielding even becomes the dominant growth mechanism. One remark about the norm. When a total kinetic energy norm is used instead of a surface kinetic energy norm (not shown here), the contribution

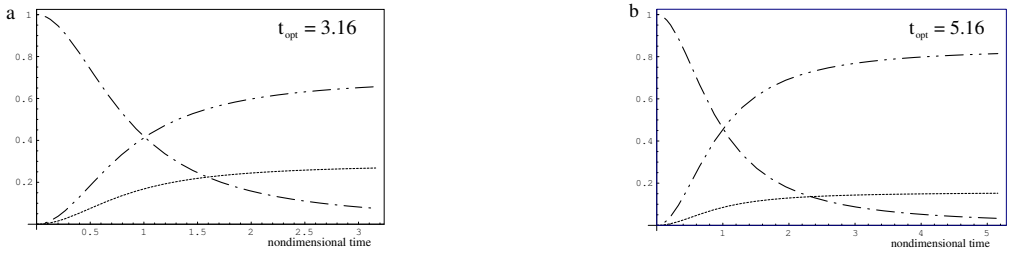

Fig. 4: The time-evolution of the projection coefficients for the (a) $t_{opt} = 3.16$ (30 hours) and (b) $t_{opt} = 5.16$ (2 days) optimal building block. Norm: surface kinetic energy. $\langle \psi_{pv}, \psi_{pv} \rangle_L / ||\psi_{sv}||^2$ (dash-dot), $2\langle \psi_{pv}, \psi_\theta \rangle_L / ||\psi_{sv}||^2$ (full) and $\langle \psi_\theta, \psi_\theta \rangle_L / ||\psi_{sv}||^2$ (dash-dot-dot).

Fig. 5: Schematic evolution of a CM-edge wave couplet (a) below and (b) above the resonant level. The large W indicates the location of the net surface warm anomaly (the lower encircled cross and dot are the wind fields around this net warm anomaly). Other symbols are the same as in Fig. 2.

of PV-PT unshielding becomes even smaller and resonance explains virtually all surface development.

Hence, what we have seen in the previous two sections is that PV-PT unshielding contributes positively to the growth due to resonance. In the next section we will illuminate how this explains the location (i.e. above the resonant level) of the optimal building block.

b. The importance of PV-PT unshielding

There is a fundamental reason for the fact that the PV anomaly above the resonant level results in a larger growth-factor than the same amplitude PV anomaly located below the resonant level. It is easily verified from (13) that the net surface PT wave that is generated moves with the mean speed of PV anomaly and Eady edge wave. As a consequence, the net surface warm anomaly which is generated a quarter wavelength downwind of the PV anomaly, tends to move under the positive PV anomaly if the PV lies above the steering level, while it tends to propagate towards the negative PV anomaly if the PV lies below the steering level. In terms of PV thinking, this implies that in the latter case the winds generated by the warm anomaly tend to cancel the winds due to PV, whereas they add up with the winds due to PV in the former case. This is

illustrated schematically in Fig. 5.

From the schematic drawings one may see that for given optimization time, the situation with maximal possible surface kinetic energy is the one where the net surface warm anomaly resides completely below the PV anomaly. This provides a theoretical upper limit for the height of the PV anomaly at

$$h = \frac{1}{\mu} + \frac{\pi}{k\Lambda t_{opt}}. \tag{15}$$

It turns out that h_{opt} lies below the upper limit for all optimization times. This implies that at optimization time the SV has not yet reached maximal amplitude. For given h_{opt}, the maximal amplitude will be obtained at time $t = k\Lambda/(\pi(h_{opt} - 1/\mu))$. The fact that actual optimal height is below the upper limit for all optimization times illustrates that there is another effect that plays a role, which is of course the resonance. First we have unshielding of ψ_{pv} and ψ_θ, which is clearly occurring more rapidly if the PV is far away from the steering level. The second effect is the resonance effect of a growing ψ_θ, which becomes stronger if the PV is located more close to the resonant level. The optimum is somewhere in between and depends on the optimization time.

c. Summary

To conclude this section, we present a short summary of the results. We have shown that resonance is the most important growth mechanism for one optimal building block. PV-PT unshielding has a secondary effect and generates significant additional growth especially for small optimization times and at the surface. For large optimization times virtually all growth is explained by the resonance.

Although the baroclinic development of one PV building block has some realistic features, the singular character of the PV anomaly must be considered as highly unrealistic. It is known that a more realistically shaped initial PV distribution will be affected by smoothing effects. For the semi-infinite Eady model, Chang (1992) mentions that non-resonance effects will dominate the dynamics in any finite-size continuous sample. Chang's study does not answer the question whether this 'finite-size' effect will enhance or diminish the perturbation growth. This will be the topic of the next section. By adding more PV building blocks to the initial perturbation, we will include PV-unshielding and study its impact on the growth.

5. Towards a SV with general PV distribution

In this section two PV anomalies at different levels are allowed in the initial perturbation. This structure is then optimized to produce a maximal growth-factor for a certain optimization time t_{opt}. However, it is easy to verify that a growth-factor based on the surface kinetic energy will run into problems because the streamfunction of two PV anomalies may cancel at one particular level. As a consequence, any optimization

algorithm generates zero initial surface kinetic energy in the search for an optimal growth-factor $\Gamma(t)$. Any nonzero final surface kinetic energy will produce an (almost) infinite growth-factor. This problem occurs already when two modes are used and will get worse when the number of modes is increased.

The problem is even worse. By looking at the structure of the initial PV anomaly and its mathematical representation ψ_{pv}^{cm} in (6), it is clear that for a suitable choice of amplitudes and initial phase-difference, the total streamfunction associated with two PV anomalies may vanish completely below the lower PV anomaly. Therefore, if one considers any kinetic energy norm, one needs to integrate over a domain that includes *at least* the levels where the PV anomalies reside. It may be for this reason that a total kinetic energy norm is used in most numerical simulations (Farrell 1989; Morgan 2001; Morgan and Chen 2002; Kim and Morgan 2002). Additionally if one determines the total energy numerically one has to be careful to choose representative levels to calculate the energy. A suitable choice seems to calculate the energy at the same levels as where the PV anomalies reside. In the Appendix, we shortly comment on another reasonable possibility which is sensitive to errors.

To overcome the above mentioned problems, an integration height of four times the Rossby height is chosen. Perturbations are expected to have died out sufficiently at this level. For the one-couplet problem the optimal height of the PV anomaly when the integrated kinetic energy is taken as a norm is located above but closer to the resonant level for all optimization times (as compared with Fig. 3). When the number of PV anomalies in the initial perturbation increases, the mathematical expression of the growth factor gets cumbersome. Fortunately, there exists an elegant technique to solve the optimization problem numerically. This is discussed below.

a. Numerical determination of the SV

The standard numerical approach to the optimization problem divides the atmosphere in M horizontal levels. The discretized, linearized dynamical operator yields M eigenvectors, which describe the modal structures supported by the basic flow. The problem with the large amplitude of the CM near the resonant level is removed by rescaling the CM to unit amplitude in some physical norm (Morgan and Chen 2002). In this way, the resonant mode is systematically excluded from the continuous spectrum and only near resonant modes are retained. Instead of using normalized modes, we use the more physically oriented PV-basis where the problem of near-singular modes does not occur. For each level $h_i \geq 0$, equation (13) describing the evolution of a PV anomaly at height h_i defines an eigenfunction $\psi(x, z, t; h_i)$ in the space of all possible perturbation structures. This eigenfunction can be represented as an M-dimensional vector $\boldsymbol{\psi}(x, z, t; h_i)$ with coefficients $[\boldsymbol{\psi}(x, z, t; h_i)]_j = \psi(x, z_j, t; h_i)$. With these eigenfunctions which serve as the basisfunctions in our PV-basis

one can construct the $M \times M$ matrix $\mathbf{X}(t)$

$$[\mathbf{X}]_{ij}(t) := \psi(x, z_i, t; h_j)$$

Any perturbation streamfunction $\boldsymbol{\psi}_{arb}$ is represented by an M-dimensional state vector. This state vector can be decomposed in the complete set of basisfunctions with appropriate projection coeffients a_i:

$$\boldsymbol{\psi}_{arb}(x, z, t) = \sum_{j=1}^{M} a_j \boldsymbol{\psi}_j(x, z, t; h_j) = \mathbf{X}(t) \cdot \boldsymbol{a}. \tag{16}$$

With the matrix of basisfunctions and the choice of the norm the numerical determination of the SV is straightforward. The functional to be maximized is known since the work of Borges and Hartmann (1992). In the present PV-basis it reads

$$\theta(\boldsymbol{a}) = \boldsymbol{a}^H \cdot \Big(\mathbf{X}(t)^H \cdot \mathbf{X}(t) \Big) \cdot \boldsymbol{a} - \lambda^2 \Big(\boldsymbol{a}^H \cdot (\mathbf{X}(0)^H \cdot \mathbf{X}(0)) \cdot \boldsymbol{a} - 1 \Big), \tag{17}$$

with A^H meaning the conjugate transpose of the object A. Setting the first variation with respect to $\boldsymbol{a}$ equal to zero, one may verify that the optimal perturbation structure is given by the eigenfunction corresponding to the largest eigenvalue λ^2 of the following eigenvalue problem

$$\Big(\mathbf{X}(0)^H \cdot \mathbf{X}(0) \Big)^{-1} \cdot \Big(\mathbf{X}(t)^H \cdot \mathbf{X}(t) \Big) \boldsymbol{a} = \lambda^2 \boldsymbol{a}, \tag{18}$$

and $\boldsymbol{\psi}(0)$ is given by $\mathbf{X}(0)\boldsymbol{a}$. The relation to the previously defined growth-factor $\Gamma(t)$ is clear. For fixed horizontal wavenumber, the total kinetic energy norm matches with the streamfunction variance norm (L2-norm) up to a constant multiplication factor. The growth-factor is the value of λ^2_{max} if instead of surface kinetic energy, the total kinetic energy is used. In fact, the above eigenvalue problem can be easily generalized to optimize for different norms, such as total quasigeostrophic energy norm or potential enstrophy norm (Kim and Morgan 2002). The solution to the eigenvalue problem determines the complex valued projection vector $\boldsymbol{a}$, and hence the amplitude and phases of the PV anomalies (CM-edge wave couplets) and the surface potential temperature of the initial perturbation.

b. Results for 2 PV anomalies

When we have two PV anomalies residing at two of the M possible interior levels, say h_1 and h_2, the matrix $\mathbf{X}(t)$ becomes $2 \times M$ dimensional. For given h_1 and h_2, the optimal structure is calculated using Eq. (18). Furthermore h_1 and h_2 are varied in height, to obtain the global maximum in parameter space (h_1, h_2). In Fig. 6 we have plotted the growth-factor for nondimensional optimization time $t_{opt} = 5.16$ (2 days) as a function of the height h_2 retaining h_1 at its global optimum. Again we see a rather sharp peak above resonant level. It may be verified that both PV anomalies lie above the resonant level and below the maximum level as defined by 15 again, similar to the SV constructed with one PV anomaly.

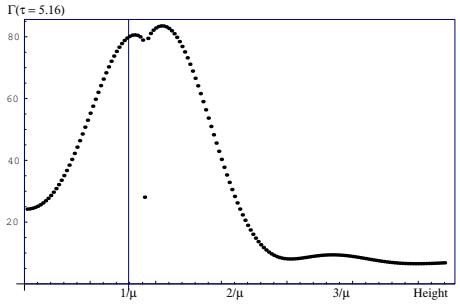

Fig. 6: Height dependence of Γ for $t_{opt} = 5.16$. h_1 is chosen to be at the optimal level and h_2 is varied to show the height dependence of the optimal solution. The isolated point just above the resonant level is the situation where the PV anomalies reside at the same height and PV-unshielding does not occur.

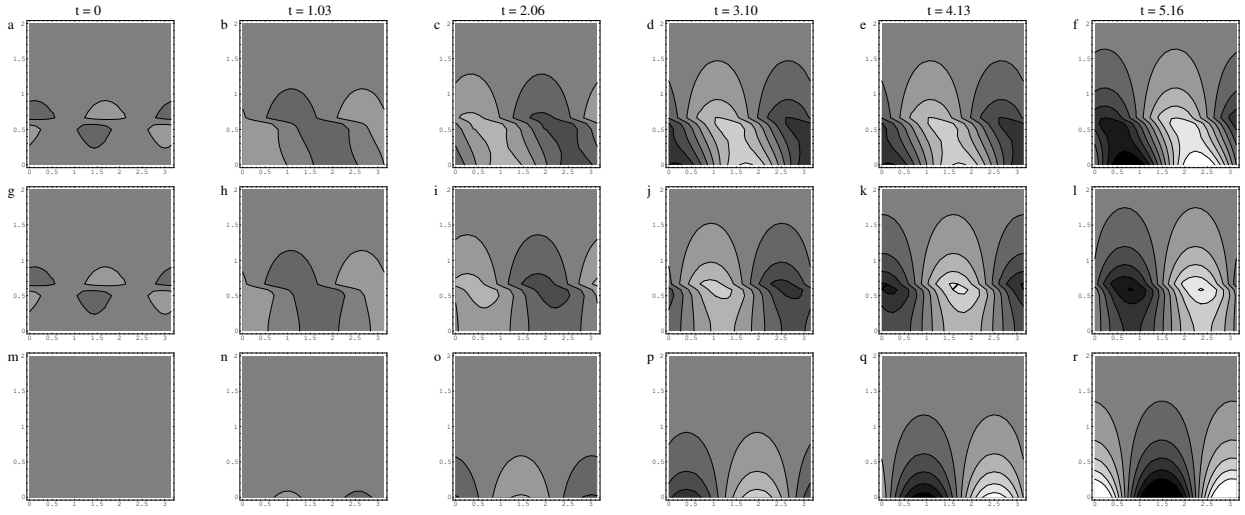

Fig. 7: Evolution of the streamfunction of the 2-couplets SV for $t_{opt} = 5.16$ and $k = 2.0$. Displayed are: (a-g) the total SV streamfunction, (h-l) the part of ψ that is associated with the PV only, and (m-r) the part of ψ that is associated with the boundary PT only. At the optimization time, the growth-factor has reached a value of 83.5. Range of contours (-1,1).

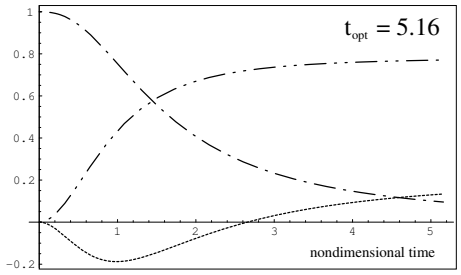

Fig. 8: The time-evolution of the surface projection coefficients for the $t_{opt} = 5.16$ SV with two PV anomalies in the initial perturbation. Norm: total kinetic energy. $(\langle\psi_{pv}, \psi_{pv}\rangle_L / ||\psi_{sv}||^{-2})|_{z=0}$ (dash-dot), $(2\langle\psi_{pv}, \psi_\theta\rangle_L ||\psi_{sv}||^{-2})|_{z=0}$ (full) and $(\langle\psi_\theta, \psi_\theta\rangle_L / ||\psi_{sv}||^{-2})|_{z=0}$ (dash-dot-dot).

The evolution of the streamfunction of the optimal perturbation is given in Fig. 7. The PV anomalies reside at optimal positions, $z = 0.566$ and at $z = 0.642$ and are almost completely out of phase initially. Therefore, the total streamfunction vanishes except in a narrow region around the positions of the anomalies (Fig. 7 a). Comparing Fig. 7 a and c, we see that the SV initially completely projects on the PV part. As time increases, the PV anomalies disperse, and the streamfunction reaches the surface (Fig. 7 h-i). The surface winds then start to advect the background gradient of potential temperature and a surface PT anomaly is generated (Fig. 7 n-r). This surface PT anomaly then quickly amplifies because of the resonance between the PV anomalies and the edge waves. At the optimization time $t = 5.16$, the surface PT wave has obtained a large amplitude and most of the surface winds in this stage are attributable to the surface temperature perturbation (compare Fig. 7 l and r).

Notice that the 2 PV anomaly problem does not evolve towards a vertical PV-tower configuration. Apparently, resonance and PV-PT unshielding is more effective than the PV-towering mechanism. The growth-factor, now defined with respect to the total kinetic energy reaches the value of 83.5 at the optimization time. To get a more quantitative insight of the surface development, we have plotted the evolution of the surface projection coefficients of the $t_{opt} = 5.16$ SV in Fig. 8 (c.f Fig. 4 of the previous section). A comparison with Fig. 4 shows that PV-PT unshielding contributes negatively to the growth in the initial stages of the surface development. In the meanwhile the effect of PV-unshielding mechanism is enhanced. Resonance still dominates the surface development at final time. Again, we do not show the results for the total (as compared to surface) projection coefficients as they resemble the evolution shown in Fig. fig:sv516str where an even more pronounced role is played by the PV-unshielding mechanism.

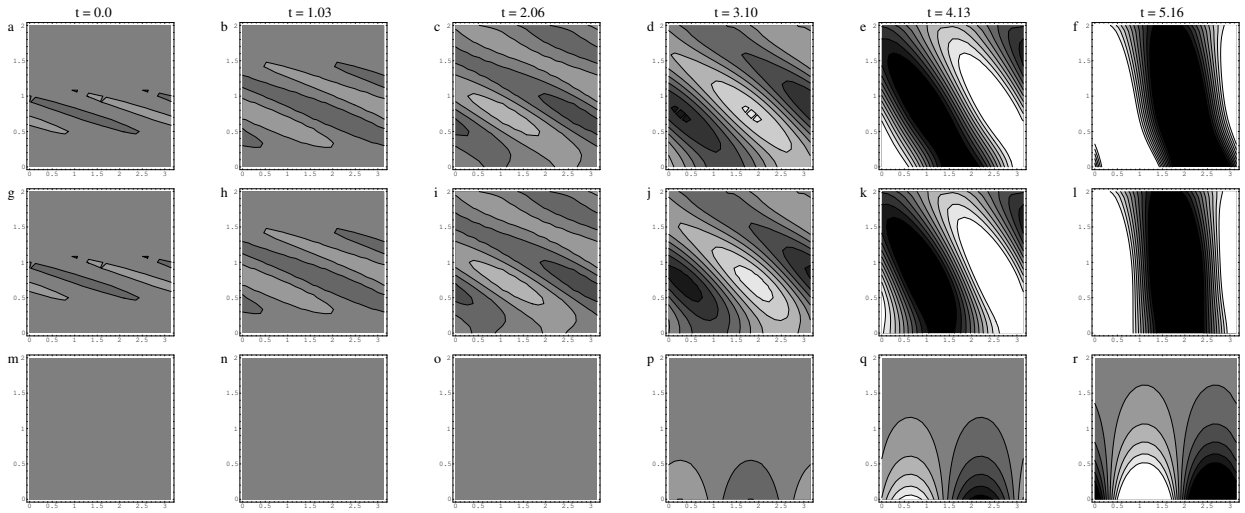

Fig. 9: Evolution of the streamfunction of the ($M = 40$)-couplets SV for $t_{opt} = 5.16$ and $k = 2.0$. Displayed are: (a-f) the total SV streamfunction, (g-l) the part of ψ that is associated with the PV only, (m-r) and the part of ψ that is associated with the surface PT only. At optimization time, the growth-factor has reached the value 622.0. Range of contours (-2,2).

c. Results for M PV anomalies

To be complete, we present here the result for $M = 40$. Again $t_{opt} = 5.16$ and the SV is constructed for the total kinetic energy norm. The evolution of the SV towards $t = t_{opt}$ and its underlying PV and PT part are displayed in Fig. 9. For the interior, PV-unshielding has become the dominant mechanism in the evolution towards $t = 5.16$. Again, we start off with a streamfunction structure that is tilted rather upshear and concentrated in a region just above the resonant level (Fig. 9a and Fig. 10a). As compared with the 2 couplets problem, it seems that it takes more time for the perturbation streamfunction to reach the surface However, for graphical reasons we have changed the contour interval here, and it is verified (not shown) that on both cases the perturbation reaches the surface almost at the same time. Once the streamfunction has reached the surface (Fig. 9c) a PT wave is rapidly developing (Fig. 9p-r). At optimization time the streamfunction attributable to the PV anomalies is almost barotropic (Fig. 9l). The corresponding PV anomalies have formed an almost vertical structure, which is displayed in Fig. 10b. This is different as compared with the previous section where the PV anomalies were still upshear tilted with height at the optimization time. In the general problem only a few levels at the top are slightly out of phase but this is not because of some fundamental reason. These top levels take into account the average influence of all levels above and they can be positioned (slightly) out of phase.

Let us now turn to the surface dynamics. In Fig. 11 we have displayed the evolution of the different surface

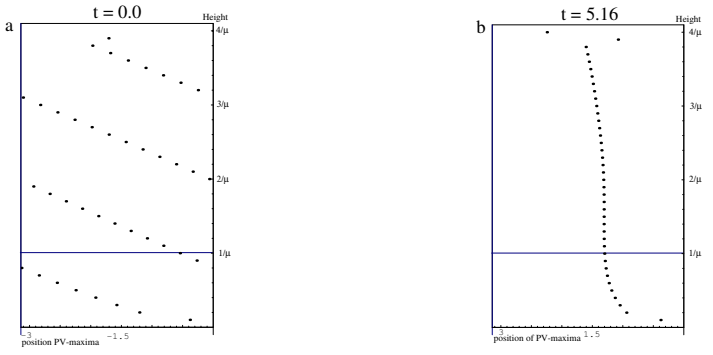

Fig. 10: (a) Initial and (b) final PV configuration for the $t_{opt} = 5.16$ SV.

Fig. 11: The time-evolution of the different surface projection coefficients for (a) the $t_{opt} = 5.16$ and (b) $t_{opt} = 10.32$ (right) SV with $M = 40$ PV anomalies. Initial norm total kinetic energy. Norm: total kinetic energy. $(\langle\psi_{pv}, \psi_{pv}\rangle_L / ||\psi_{sv}||^{-2})|_{z=0}$ (dash-dot), $(2\langle\psi_{pv}, \psi_\theta\rangle_L ||\psi_{sv}||^{-2})|_{z=0}$ (full) and $(\langle\psi_\theta, \psi_\theta\rangle_L / ||\psi_{sv}||^{-2})|_{z=0}$ (dash-dot-dot).

Fig. 12: Amplitudes of the PV-maxima for (a) the $t_{opt} = 5.16$ SV and (b) $t_{opt} = 10.32$ SV.The anomalous large amplitude of the PV at the two topmost levels is the effect of truncating the vertical domain at $z = 4/\mu$, and in some sense summarized the mean effect of all modes above that level.

projection coefficients for two different optimization times. Something unexpected seems to be happening at the surface in the initial stages of the development (Fig. 11a). However, a close inspection would show that the surface projection coefficients explode because the SV streamfunction vanishes at the surface because PV-PT unshielding counteracts surface development due to PV-superposition. Hence, the rapid surface cyclogenesis occuring roughly after $t = 1$ is preceded by rapid surface cyclolysis. This is perfectly possible as we chose total kinetic energy as an optimization norm. After this initial weakening of the surface winds, at $t \sim 4.2$ the resonance clearly takes over the surface development which is initially mostly due to PV-unshielding. PV-PT unshielding contributes negatively to to the surface development during almost the complete time-evolution. Increasing the optimization time (Fig. 11b) to four days leads to similar results for the surface development as we saw before in the case with one or two PV anomalies (Fig. 8); resonance becomes increasingly more important.

Yet another way to illustrate the importance of resonance in the general problem is to consider the distribution of PV in the vertical. In Fig. 12, we displayed the amplitudes of the PV at specific levels for the $t_{opt} = 5.16$ (2 days) and $t_{opt} = 10.32$ (4 days) SV. These figures looks similar to Fig. 3 although in Fig. 3 we have plotted the growth-factor as function of the height of the PV anomaly. We see that for $t_{opt} = 5.16$ the largest amplitudes of PV are typically observed in a rather wide domain above the resonant level. This is in line with the observation that during the complete time evolution the interior SV is dominated by growth due to PV-superposition and not due to resonance. The resonance effect is already more important for a doubled optimization time. Now, we see a rather sharp peak in a small region above the resonant level, and we expect that an even more significant part of the development will be due to resonance, which is confirmed by looking at Fig. 11b.

6. Concluding remarks

In this paper we have discussed what the effect of resonance and potential vorticity (PV) unshielding is in the evolution of the SV of the Eady model without the upper rigid lid. For this we used the PV perspective to construct a set of nonmodal basisfunctions. These basisfunctions initially have PV at some specific level and zero surface potential temperature (PT). A finite surface surface PT wave is generated as time increases. The surface PT wave and the interior PV wave may interact through the mean flow.

The nonmodal basis allowed a number of initial value experiments, in which the number of interior PV anomalies (PV building blocks) in the initial perturbation is gradually increased. Gradually increasing the complexity of the initial perturbation structure has the advantage that different growth-mechanisms can be more easily distinguished than would be the case in a completely general analysis. These mechanisms are PV-unshielding, PV-PT unshielding and resonance (a growing surface PT wave). Additionally, problems with the near singular behavior of the continuum modes (CM) near one Rossby height are avoided in this approach.

When there is only one PV anomaly in the interior, the optimal position of this PV anomaly is found in a region above the steering level of the Eady edge wave. The largest part of this growth is caused by the resonance between the PV anomaly and the surface edge wave. This resonance yields a rapidly growing surface PT-wave. However, we showed that only above the steering level, PV-PT unshielding contributes positively to the growth due to the resonance. PV-unshielding does not occur. Therefore, to include PV-unshielding as a growth mechanism, we added more PV-anomalies in the initial perturbation. We showed that PV unshielding becomes the dominant growth mechanism for the interior when the number of PV anomalies gets larger than two and when we optimized for a total kinetic energy. However, resonance is still the dominant mechanism for the surface development. For long optimization times, the PV distribution becomes rather peaked just above the steering level of the edge wave, which illustrates the enhanced importance of resonance as compared with short optimization times.

Let us finish with some remarks. First, the results of the above study suggest that atmospheric cross-sections with high vertical resolution are required to determine whether or not rapid surface cyclogenesis will occur. This resolution starts to be important especially when the time-scale exceeds more than three days as resonance only occurs around the steering levels of the neutral edge waves.

Another point that should be mentioned concerns the horizontal wavelength of the perturbations. The model is easily generalized to include a variable zonal wavenumber. If only zonally periodic solutions, this offers a mechanism of wave-number selection. Given the optimization norm and the optimization time t_{opt}, the SV will select the appropriate wavelength itself. This wave-number selection mechanism is topic of current research.

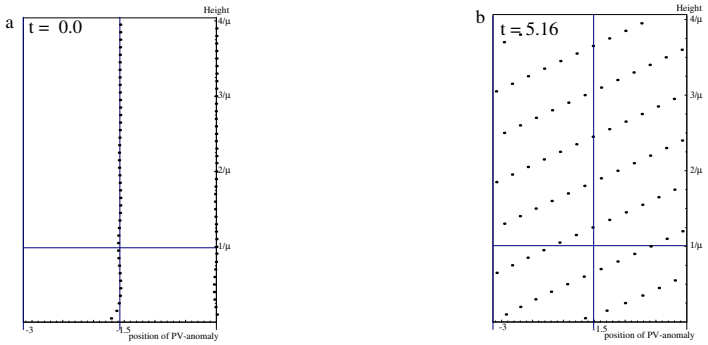

Fig. 13: Initial and final position of the PV-maxima for the $t_{opt} = 5.16$ SV calculated with a different method.

Finally, we will comment on the choice of norm here. We have chosen equal norms at initial and final time. However, this need not be done. Another interesting possibility could be to choose initially a total kinetic or total quasigeostrophic energy norm and finally a surface kinetic energy norm. It is a subject of current research to investigate whether this will changes the results in a fundamental way.

Acknowledgments

The authors wish to thank Dr. A.J. van Delden for useful discussions and remarks during the various stages of the research.

A Spurious optimal perturbations for different discretizations

In section 5. we used a particular discretization for the calculation of the total kinetic energy. The energy is calculated at the same levels as where the PV is specified. Although this is a standard approach and is done in most numerical studies, there is no *a priori* reason, why one should use this discretization. In this appendix, we therefore consider a different approach where the energy is calculated from the levels in between the levels where PV is specified. We study the M-couplet problem, with all further specifications and assumptions equal to the ones of section 5. The results for the phases of the initial PV distribution are given in Fig. 13. One observation is that the initial and final phases show a rather dramatic difference as compared to the initial and final phases of Fig. 10. Instead of being upshear tilted, we now get a phase distribution, where all subsequent couplets lie one half of a wavelength out of phase. That is, they competely mask each other, similar to the result of the two couplet problem in section 5. The question that rises is why the singular vector have this particular 'unphysical' structure. This has to do with the vertical structure around two nearby PV anomalies. It turns out, that the streamfunction in between two PV anomalies is canceled very effectively, when those

modes are one half of a wavelength out of phase. Therefore, by choosing the structure of Fig. 13, the system minimized the initial kinetic energy very effectively. To ensure unit initial kinetic energy, the amplitudes of PV at the levels have to increase enormously, which is observed.

As a conclusion it is mentioned that one has to be careful in calculating the kinetic energy at levels which are representative for the whole layer. As is clear from the above discussion, the levels in between the PV anomalies are not suitbable, and the singular vector optimization yields an unphyisical optimal perturbation.

References

Badger, J. and B. J. Hoskins, 2001: Simple initial value problems and mechanisms for baroclinic growth. *Journal of the Atmospheric Sciences*, **58**, 38–49.

Bishop, C. H. and E. Heifetz, 2000: Apparent absolute instability and the continuous spectrum. *Journal of the Atmospheric Sciences*, **57**, 3592–3608.

Borges, M. D. and D. L. Hartmann, 1992: Barotropic instability and optimal perturbations of observed nonzonal flows. *Journal of the Atmospheric Sciences*, **49**, 335–353.

Chang, E. K. M., 1992: Resonating neutral modes of the Eady model. *Journal of the Atmospheric Sciences*, **49**, 2452–2463.

Davies, H. C. and C. H. Bishop, 1994: Eady edge waves and rapid development. *Journal of the Atmospheric Sciences*, **51**, 1930–1946.

Eady, E. T., 1949: Long waves and cyclone waves. *Tellus*, **1**, 33–52.

Farrell, B. F., 1982: The initial growth of disturbances in a baroclinic flow. *Journal of the Atmospheric Sciences*, **39**, 1663–1686.

Farrell, B. F., 1984: Modal and non-modal baroclinic waves. *Journal of the Atmospheric Sciences*, **41**, 668–673.

Farrell, B. F., 1988: Optimal excitation of neutral Rossby waves. *Journal of the Atmospheric Sciences*, **45**, 163–172.

Farrell, B. F., 1989: Optimal excitation of baroclinic waves. *Journal of the Atmospheric Sciences*, **46**, 1193–1206.

Fischer, C., 1998: Linear amplification and error growth in the 2D Eady problem with uniform potential vorticity. *Journal of the Atmospheric Sciences*, **55**, 3363–3380.

Hakim, G. J., 2000: Role of nonmodal growth and nonlinearity in cyclogenesis initial-value problems. *Journal of the Atmospheric Sciences*, **57**, 2951–2967.

Hoskins, B. J., M. E. McIntyre, and A. W. Robertson, 1985: On the use and significance of isentropic potential vorticity maps. *Quarterly Journal of the Royal Meteorological Society*, **111**, 877–946.

Kim, H. M. and M. C. Morgan, 2002: Dependence of singular vector structure and evolution on the choice of norm. *Journal of the Atmospheric Sciences*, **59**, 3099–3116.

Morgan, M. C., 2001: A potential vorticity and wave activity diagnosis of optimal perturbation evolution. *Journal of the Atmospheric Sciences*, **58**, 2518–2544.

Morgan, M. C. and C. C. Chen, 2002: Diagnosis of optimal perturbation evolution in the Eady model. *Journal of the Atmospheric Sciences*, **59**, 169–185.

Mukougawa, H. and T. Ikeda, 1994: Optimal excitation of baroclinic waves in the Eady model. *Journal of the Meteorological Society of Japan*, **72**, 499–513.

Orr, W., 1907: Stability or instability of the steady-motions of a perfect liquid. *Proceedings of the Royal Irish Academy*, **27**, 9–138.

Pedlosky, J., 1964: An initial value problem in the theory of baroclinic instability. *Tellus*, **16**, 12–17.

Rotunno, R. and M. Fantini, 1989: Petterssen's "Type B" cyclogenesis in terms of discrete, neutral Eady modes. *Journal of the Atmospheric Sciences*, **46**, 3599–3604.

Thorncroft, C. D. and B. J. Hoskins, 1990: Frontal cyclogenesis. *Journal of the Atmospheric Sciences*, **47**, 2317–2336.